NANO LETTERS

pubs.acs.org/NanoLett Letter

Electrical Switching of Optical Gain in Perovskite Semiconductor Nanocrystals

Zhengyuan Qin, Chunfeng Zhang,* Lan Chen, Tao Yu, Xiaoyong Wang, and Min Xiao

Cite This: *Nano Lett.* 2021, 21, 7831−7838 Read Online

ACCESS | Metrics & More | Article Recommendations | Supporting Information

ABSTRACT: Perovskite semiconductor nanocrystals are promising for optical amplification and laser applications benefiting from efficient optical gain generation. Nevertheless, the pump threshold is limited by more than one exciton per nanocrystal required to generate population inversion in neutral nanocrystals due to the level degeneracy. Here, we show that by charging nanocrystals with current injection, the level degeneracy can be lifted to generate charged exciton gain with markedly low excitation density. On the basis of the scenario, we have demonstrated electrical switching of amplified spontaneous emission in films of $CsPbBr_3$ nanocrystals sandwiched by two electrodes with over 50% threshold reduction owing to charged excitons. Our work provides an effective approach to electrically modulated optical gain in colloidal perovskite nanocrystals for potential applications in advanced laser and information technology.

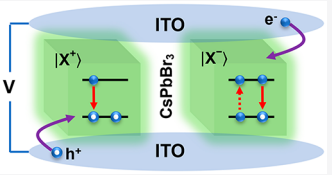

KEYWORDS: *Perovskite semiconductors, optical gain, charged exciton, electrical switching, ultrafast spectroscopy*

Lead halides of perovskite lattices have emerged as a family of semiconductors promising for optoelectronic applications.[1−19] Nanocrystal structures can further improve the strength of light−matter interaction benefiting from the quantum confinement effect.[20−31] Highly efficient light absorption and emission make perovskite semiconductor nanocrystals ideal gain media for laser demonstration.[29,32−37] Nevertheless, the inherent degeneracies of band-edge states require a relatively high pump threshold of more than one exciton per nanocrystal to achieve the population inversion to support optical gain in these nanocrystals.[38−41]

In practice, modulating and switching optical gain is of particular importance for pulse laser operation and optical telecommunication. For self-assembly quantum dots of III−V semiconductors, broad bandwidth of modulated lasers has been available as a fundamental element for next-generation optoelectronic and information technology.[42,43] It remains unclear whether optical gain switching is feasible in colloidal quantum dots. By charging nanocrystals electrically or chemically,[38,44,45] the band-edge state degeneracy can be lifted to reduce the pump threshold with charged exciton gain.[38,41,45−47] Recently, Yu et al. have shown that the amplified spontaneous emission (ASE) from II−VI chalcogenide nanocrystals can be controlled by an external electrical field.[48] ASE threshold is reduced by 10% via implanting the gain of charged excitons with applied voltage across the nanocrystal films. In comparison to the chalcogenide semiconductors, lead halides are more susceptible to the electrical field for charge injection and ion migration,[39,49−53] which is manifested as field dependence of photoluminescence emission from single $CsPbBr_3$ nanocrystals.[54] In principle, such a field effect may modulate the threshold of optical gain in perovskite semiconductor nanocrystals by introducing charged excitons, which, however, remains unexplored.

In this work, we demonstrate the electrical switching of optical gain using charged exciton gain in a device with $CsPbBr_3$ nanocrystals sandwiched between two ITO substrates. By application of an external dc voltage of 20 V, ASE from the nanocrystal film has been switched for multiple ON/OFF cycles at ambient environment. The gain switching behavior can be ascribed to ∼50% threshold reduced by charged excitons as verified by ultrafast transient absorption (TA) spectroscopy. The time-dependent measurements suggest that charged excitons are mainly introduced by charge injection and halide vacancy diffusion. The findings demonstrate the proof of principle for gain switching with charged excitons which may stimulate applications of perovskite nanocrystals in next-generation optoelectronic devices.

Figure 1 shows the scenario for gain switching based on charged exciton gain in this work. The band-edge states of perovskite semiconductor nanocrystals are 2-fold degenerated (i.e., $g_e = g_h = 2$)[55] so that the cross sections of absorption and stimulated emission in singly excited nanocrystal are offset for neutral nanocrystals (Figure 1a). Optical gain can be generated with stimulated emission from biexciton ($|XX\rangle$) states under relatively high-density pumping. While in single-charged nanocrystals (Figure 1b), the absorption of a single photon

Received: July 26, 2021
Published: September 7, 2021

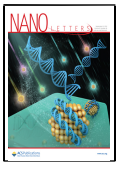

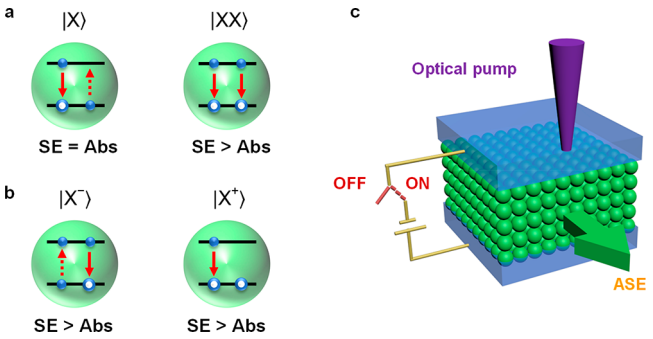

Figure 1. Schematic diagram for optical gain switching based on charged excitons. (a) In neutral nanocrystals, optical gain can be generated only when more than one exciton per nanocrystal is excited. (b) In charged nanocrystals, both negatively and positively charged excitons may contribute to optical gain at the single excitation level. (c) The device consists of the nanocrystal film sandwiched by two ITO electrodes for optical gain switching.

forms a charged exciton (either a negative or a positive trion), resulting in optical gain generation as the additional charge lifts the degeneracy of electron/hole level for negative/positive trions.[38] In principle, an external electric field may switch on the optical gain from singly excited perovskite nanocrystals. We employ a simple device structure by sandwiching a nanocrystal layer with two ITO electrodes where the nanocrystals are expected to be charged by applying an external voltage at the two electrodes (Figure 1c).

Figure 2a and Figure 2b show the edge emission spectra from the nanocrystal film under pump at 400 nm of 40 μJ/cm^2 with several cycles with/without applying an external voltage of 20 V. Without an applied external field, PL spectra exhibit broadband spontaneous emission centered at 520 nm with a line width of ~25 nm. With an applied external field, a pronounced sharp peak at 535 nm with a line width of <4 nm emerges. The results demonstrate the switching of optical gain with the applied external field. The optical gain is switched ON as manifested with the pronounced ASE emission at 535 nm while the spontaneous emission is suppressed (Figure 2c). No significant degradation was detected at ambient environment after several cycles of ON/OFF switching, implying the promising potential for the device stability.

The gain switching behavior can be explained as the charging induced threshold reduction. Figure 2d and Figure 2e compare the pump-fluence-dependent PL spectra from the device without and with applying an external field of 20 V, respectively. Due to the gain-induced narrowing, ASE has been detected from the device for both configurations when the pump fluence exceeds the thresholds (inset, Figure 2d and Figure 2e, Figure S2). Notably, the pump threshold of ASE shows strong dependence on the applied voltage, decreasing from 68 μJ/cm^2 to 32 μJ/cm^2 when the external field increases from 0 to 20 V (Figure 2f). With further increasing of the applied voltage, the possibility of device breakdown increases. The threshold is higher than the literature values in optimized neat films, which is likely caused by the loss at the nanocrystal/electrode interfaces and the relatively high refractive index of ITO glass. Nevertheless, more than 50% of threshold reduction induced by the external field results in the gain switching behavior.

We performed transient absorption (TA) spectroscopic measurements on a film of $CsPbBr_3$ nanocrystals to study the dynamics of gain generation in these samples with different pump densities (Figures S3 and S4). The pump density, in term of average number of excitations per nanocrystal ($\langle N \rangle$), is evaluated assuming Poisson distribution of absorbed photons (Figure S5). For transmission measurements, a film sample with optical density of ~0.46 (~150 nm thick) is sandwiched between two transparent electrodes with application of an external electric field of 20 V to modulate the optical gain. The TA signal consists of multiple components, including a major band of the ground-state bleaching (GSB) at the band edge, the stimulated emission (SE), and the excited-state absorption (ESA) (Figure S3). Notably, the optical gain appears in the wavelength range of 530−540 nm with increasing pump fluence (Figure 3a and Figure 3b). With increasing pump density, the gain is manifested with a crossover to negative absorption in the spectral range right below the bandgap (Figure 3a and Figure 3b). With application of the electrical field, the optical gain threshold in terms of $\langle N \rangle$ decreases to the level of ~0.5 from ~1 recorded without applying the field as expected for charged exciton gain (Figure 3c). The spectral peak of optical gain is ~2 nm shorter in the sample with the external field than that in the sample without the field. The energy difference is ~8 meV, which is comparable to the difference between the binding energies of charged excitons and biexcitons.[56] The spectral difference is not as significant as observed in the microcrystalline film,[57] which is likely caused by the inhomogeneous line width broadening effect for nanocrystals with size diversity.[58]

The feature of charged exciton gain is also manifested in the kinetics which has been analyzed using multiexponential decay functions (Table S1). Figure 3d shows the kinetic curves of GSB signals with a low fluence pump ($\langle N \rangle$ = 0.06) for the samples with and without applied voltage. With application of the electrical field, the amplitude of GSB signal is markedly reduced and an additional fast decay component emerges with a lifetime of ~290 ps, which is consistent with the behavior of charged excitons.[55,59] With application of the external field, the amplitude of the bleach signal (Figure 3d) drops significantly, which is a consequence of electrical doping. By charging the nanocrystals, the excitonic absorption at the absorption edge is reduced due to the field-induced charges occupied at the excited states. Stimulated emission from charged exciton is off resonant to the exciton transition. Both effects result in the observed drop of bleaching signal in the film with applying external field. With increasing $\langle N \rangle$ to ~0.7 above the threshold, the dynamics of SE at 537 nm recorded from the charged sample is dominated by a decay component with the lifetime of ~290 ps (Figure 3e), which is not largely sensitive to the pump density (inset, Figure 3e). These results strongly support that the SE from charge excitons makes the dominant contribution to the optical gain generation in the charged film. In contrast, the optical gain in the uncharged film is mainly contributed by a component of ~80 ps with pump density above the threshold (Figure 3f). The fast decay component, only present at high excitation density regime (inset, Figure 3f), is mainly induced by the biexciton effect. That is, more than one exciton is required to generate optical gain in neutral nanocrystals. The recombination lifetime of charged exciton is much longer than that of biexciton, resulting a longer lifetime for charge exciton gain. The lifetime of charged exciton gain is ~220 ps with $\langle N \rangle$ = 0.7 in the film with application of the external field, which is much longer than the biexciton gain of ~24 ps with $\langle N \rangle$ = 1.2 in the film without application of the external field. The relatively low pump density required for population inversion and the long lifetime for charged exciton gain result in low pump threshold, enabling the gain switching under the external field.

https://doi.org/10.1021/acs.nanolett.1c02880
Nano Lett. 2021, 21, 7831−7838

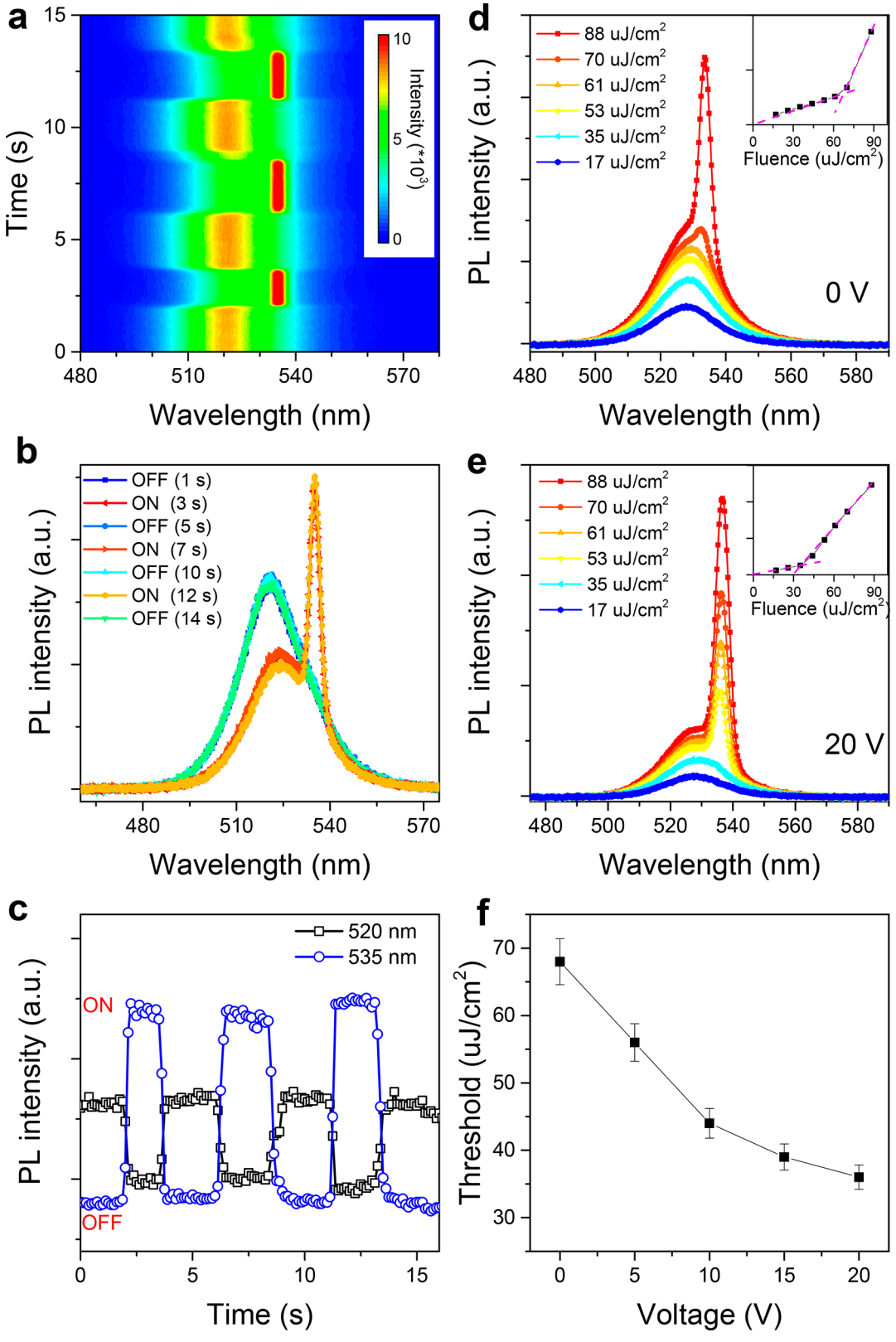

Figure 2. Electrical switching of optical gain. (a) Time-dependent emission spectra recorded continuously under several cycle switching with the applied voltage of 20 V. (b) Typical emission spectra recorded at different times for the ON and OFF states. (c) Time-dependent PL emission intensities at the wavelengths of 520 and 535 nm. Pump-fluence-dependent PL spectra of the $CsPbBr_3$ nanocrystal film (d) without and (e) with applied voltages. (f) The ASE threshold is plotted as a function of the applied voltage. The emission spectra were recorded with pump fluence of 40 $\mu J/cm^2$ at 400 nm.

In principle, more complex excitations, such as charged biexcitons or doubly charged excitons, may also be optically excited. It is difficult to distinguish charged biexcitons and biexcitons from the TA kinetics. Fortunately, neither of them

https://doi.org/10.1021/acs.nanolett.1c02880
Nano Lett. 2021, 21, 7831−7838

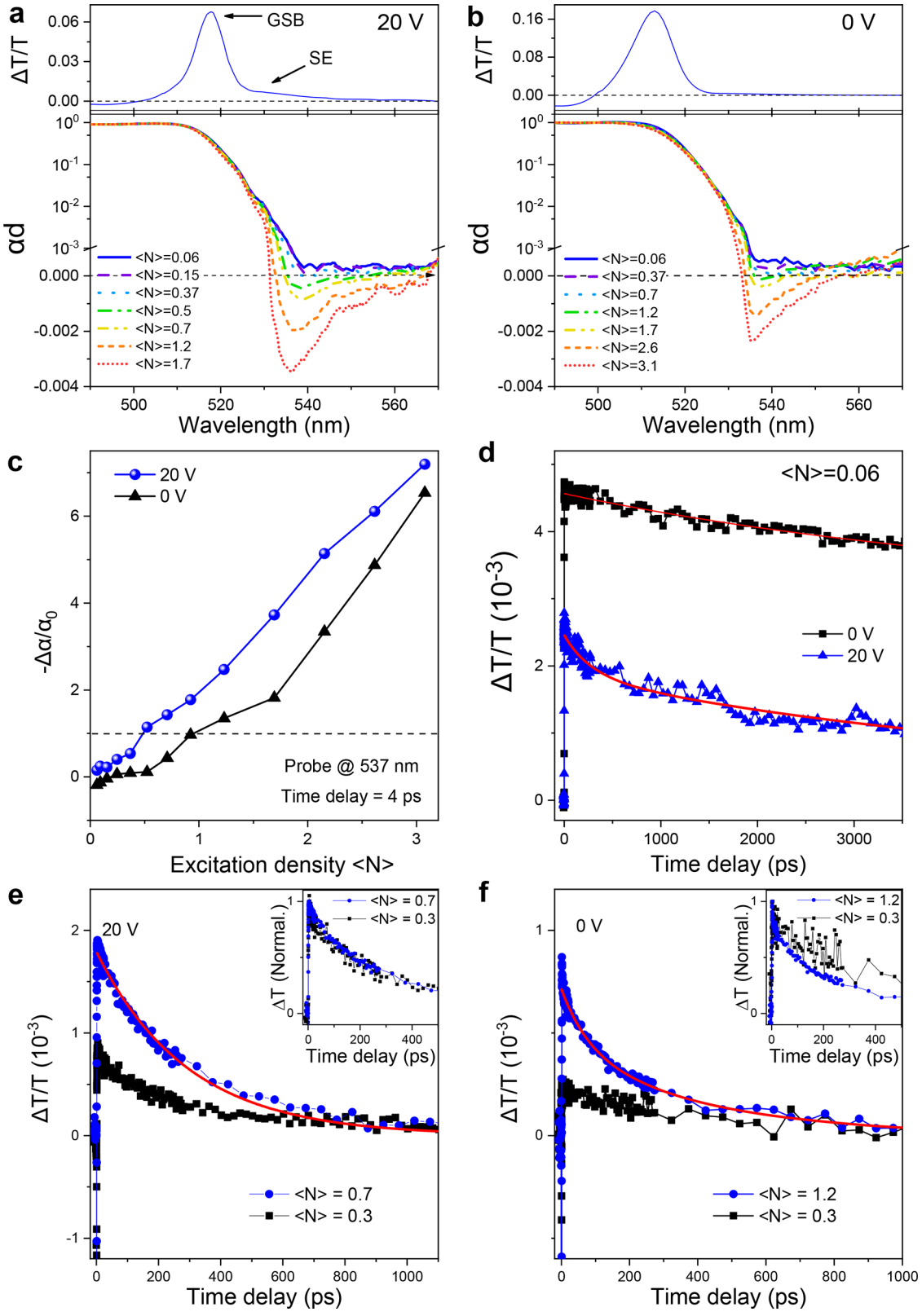

Figure 3. TA spectroscopic study of gain mechanism. Absorption spectra of a thin film sample of $CsPbBr_3$ nanocrystals (a) with and (b) without application of a voltage of 20 V with pump of different excitation densities ($\langle N \rangle$). αd stands for optical density where α is the absorption coefficient and d is the optical path length, respectively. TA spectra are shown for references. The spectra are recorded at a time delay of 4 ps. (c) The optically induced absorption changes ($-\Delta\alpha/\alpha_0$) are plotted versus pump density ($\langle N \rangle$). The data are probed at 537 nm and a time delay of 4 ps. (d) Kinetic curves of GSB signals probed at 518 and 514 nm for the samples with and without application of the external voltage, respectively. The traces were recorded with pump of a low pump fluence ($\langle N \rangle = 0.06$). The TA kinetics probed at 537 nm with the pump fluences below and above the ASE thresholds for the samples with (e) and without (f) application of the external voltage. Insets show the normalized signals.

https://doi.org/10.1021/acs.nanolett.1c02880
Nano Lett. 2021, 21, 7831−7838

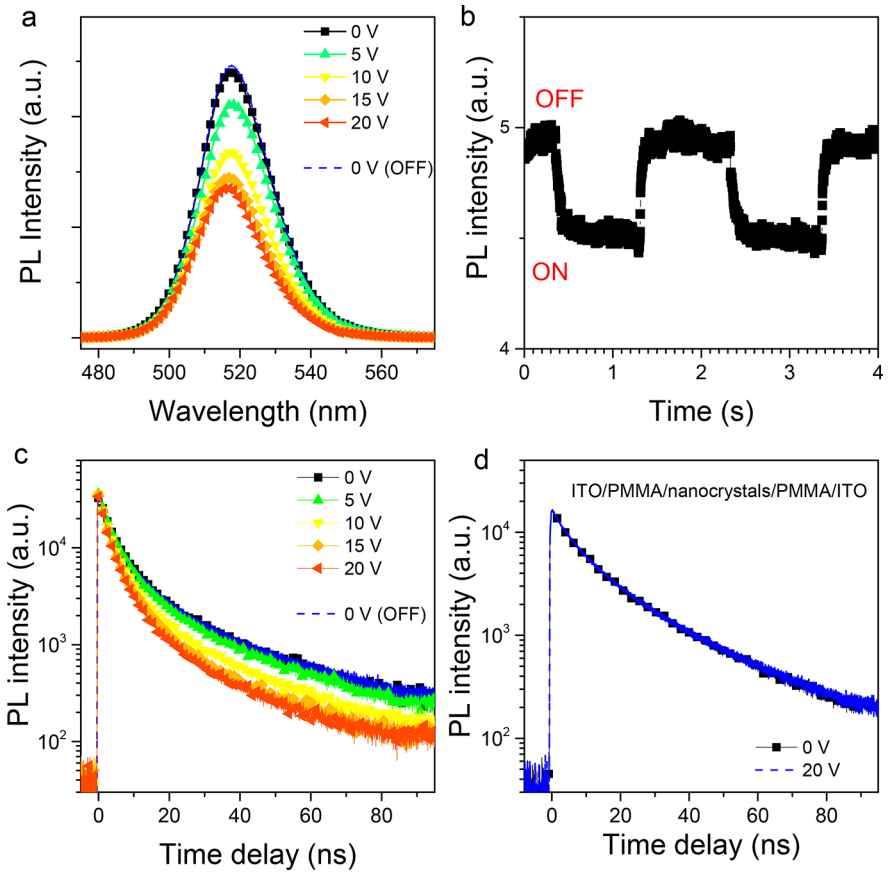

Figure 4. Electrical field modulation of PL emission. (a) PL emission spectra recorded with different applied voltages. (b) PL intensity of the sample under cw excitation modulated by a periodic voltage at a frequency of 0.5 Hz. The response time of PL change is faster than 0.1 s. (c) Time-resolved PL spectra recorded with different applied voltages. (d) Time-resolved PL spectra of a sample with PMMA embedded between the electrode and nanocrystal films. In the sample, PL dynamics is not sensitive to the applied voltage.

plays a major role with pump fluence of $\langle N \rangle$ = 0.7. Doubly charged nanocrystals may also be formed with charge injection under the applied electric field. We check PL emission at the different level of current injection (Figure S6). The data suggest that double charging is insignificant as also observed in CdSe nanocrystals.[46] Possibly, singly charged nanocrystals become more difficult to be doubly charged via applying voltage due to Coulomb repulsion effect. In addition, the charge migration in the perovskite semiconductors may mitigate the charge accumulation.

The charging effect is also manifested with the dynamics of spontaneous emission (Figure 4a). When the ASE is switched ON, the intensity of spontaneous emission is markedly reduced (Figure 2b and Figure 2c). For more insights, we recorded time-integrated and time-resolved PL spectra from the sample with application of external field of different voltages. The pump density is set at a very weak level (2 nJ/cm^2) which is far below the ASE threshold. As the applied voltage increases, PL intensity gradually decreases and PL decay becomes faster. Moreover, both PL intensity and decay lifetime recover when the applied voltage is withdrawn, suggesting that the charging is a reversible process. Microscopically, multiple origins should be involved in the process of charging nanocrystals including the interfacial charge injection, halide or cation vacancy diffusion, and ion accumulation.[39,49−52] Previous studies suggest that these effects occur on different time scales.[49] To characterize the response time of charging process, we recorded the PL emission integrated over 10 ms under cw laser excitation modulated by a periodic voltage at a frequency of 0.5 Hz. As shown in Figure 4b, the response time of PL change is shorter than 100 ms, which is much faster than the processes of ion accumulation and cation vacancy diffusion with typical time scales longer than 1 s. These results imply that the charging is mainly induced by the charge injection at the electrode/nanocrystal interface and the halide vacancy diffusion inside the nanocrystal film. The nonradiative recombination channel caused by the vacancy diffusion, together with the nonradiative Auger recombination of charged excitons, is probably responsible for faster PL decay in charged samples (Figure 4c).

In addition to the charge injection, the electric field may modulate the optical response of a semiconductor through the Stark effect.[60,61] Such a field-induced Stark effect does not rely on the electrode/nanocrystal contact in principle. To isolate the Stark effect, we introduce thin layers of poly(methyl methacrylate) (PMMA) of ∼20 nm between the ITO and nanocrystal layers which insulate direct charge injection. In such a sample, PL emission is no longer sensitive to the applied voltage up to 20 V (Figure 4d), confirming that the charge injection is the primary cause of optical gain switching. Moreover, the heating effect caused by the current injection may also modify PL emission, which deserves more in-depth research in the future. To minimize the side effect, we have synchronized the external field with the pump laser and kept the measurements in short time in our work.

In summary, we have demonstrated the proof of principle for electrical switching of optical gain in perovskite semiconductor

https://doi.org/10.1021/acs.nanolett.1c02880
Nano Lett. 2021, 21, 7831−7838

nanocrystals by employing the charged excitons. The carrier dynamics in $CsPbBr_3$ nanocrystal films are determined by the interplay between excitons, charged excitons, and biexcitons. When the external field is applied, the charged excitons make the most significant contribution to the optical gain generation under low excitation density. Remarkably, by lifting the level degeneracy, optical gain from charged excitons is achievable with markedly lower excitation density than that from biexcitons, enabling the optical gain switching in perovskite nanocrystals. The operation threshold for the current device is not optimized due to the high refractive index of ITO electrodes and the roughness at the electron/nanocrystal interface. These imperfections can be potentially addressed by structure design especially with monolithic integration using substrates with low refractive index. The findings show a feasible approach to electrically modulating optical gain in perovskite nanocrystals, which may facilitate the exploration of using colloidal perovskite nanocrystals in advanced laser and information technology.

■ ASSOCIATED CONTENT

Supporting Information

The Supporting Information is available free of charge at https://pubs.acs.org/doi/10.1021/acs.nanolett.1c02880.

Experimental details of sample synthesis, device fabrication, and optical characterization; quantification of excitation density; electrode contact characterization (PDF)

■ AUTHOR INFORMATION

Corresponding Author

Chunfeng Zhang − *National Laboratory of Solid State Microstructures, School of Physics, and Collaborative Innovation Center for Advanced Microstructures, Nanjing University, Nanjing 210093, China;* orcid.org/0000-0001-9030-5606; Email: cfzhang@nju.edu.cn

Authors

Zhengyuan Qin − *National Laboratory of Solid State Microstructures, School of Physics, and Collaborative Innovation Center for Advanced Microstructures, Nanjing University, Nanjing 210093, China*

Lan Chen − *National Laboratory of Solid State Microstructures, School of Physics, and Collaborative Innovation Center for Advanced Microstructures, Nanjing University, Nanjing 210093, China*

Tao Yu − *National Laboratory of Solid State Microstructures, School of Physics, and Collaborative Innovation Center for Advanced Microstructures, Nanjing University, Nanjing 210093, China;* orcid.org/0000-0003-1981-3469

Xiaoyong Wang − *National Laboratory of Solid State Microstructures, School of Physics, and Collaborative Innovation Center for Advanced Microstructures, Nanjing University, Nanjing 210093, China;* orcid.org/0000-0003-1147-0051

Min Xiao − *National Laboratory of Solid State Microstructures, School of Physics, and Collaborative Innovation Center for Advanced Microstructures, Nanjing University, Nanjing 210093, China; Department of Physics, University of Arkansas, Fayetteville, Arkansas 72701, United States*

Complete contact information is available at: https://pubs.acs.org/10.1021/acs.nanolett.1c02880

Notes

The authors declare no competing financial interest.

■ ACKNOWLEDGMENTS

This work is supported by the National Key R&D Program of China (Grants 2018YFA0209101 and 2017YFA0303700), the National Science Foundation of China (Grants 21922302, 21873047, 11904168, 91833305, and 91850105), and the Fundamental Research Funds for the Central University.

■ REFERENCES

(1) Tan, Z.-K.; Moghaddam, R. S.; Lai, M. L.; Docampo, P.; Higler, R.; Deschler, F.; Price, M.; Sadhanala, A.; Pazos, L. M.; Credgington, D.; et al. Bright light-emitting diodes based on organometal halide perovskite. *Nat. Nanotechnol.* **2014**, *9*, 687−692.

(2) Cho, H.; Jeong, S.-H.; Park, M.-H.; Kim, Y.-H.; Wolf, C.; Lee, C.-L.; Heo, J. H.; Sadhanala, A.; Myoung, N.; Yoo, S.; et al. Overcoming the electroluminescence efficiency limitations of perovskite light-emitting diodes. *Science* **2015**, *350*, 1222−1225.

(3) Xiao, Z.; Kerner, R. A.; Zhao, L.; Tran, N. L.; Lee, K. M.; Koh, T.-W.; Scholes, G. D.; Rand, B. P. Efficient perovskite light-emitting diodes featuring nanometre-sized crystallites. *Nat. Photonics* **2017**, *11*, 108−115.

(4) Cao, Y.; Wang, N.; Tian, H.; Guo, J.; Wei, Y.; Chen, H.; Miao, Y.; Zou, W.; Pan, K.; He, Y.; Cao, H.; Ke, Y.; Xu, M.; Wang, Y.; Yang, M.; Du, K.; Fu, Z.; Kong, D.; Dai, D.; Jin, Y.; Li, G.; Li, H.; Peng, Q.; Wang, J.; Huang, W. Perovskite light-emitting diodes based on spontaneously formed submicrometre-scale structures. *Nature* **2018**, *562*, 249−253.

(5) Lin, K.; Xing, J.; Quan, L. N.; de Arquer, F. P. G.; Gong, X.; Lu, J.; Xie, L.; Zhao, W.; Zhang, D.; Yan, C.; Li, W.; Liu, X.; Lu, Y.; Kirman, J.; Sargent, E. H.; Xiong, Q.; Wei, Z. Perovskite light-emitting diodes with external quantum efficiency exceeding 20%. *Nature* **2018**, *562*, 245−248.

(6) Kojima, A.; Teshima, K.; Shirai, Y.; Miyasaka, T. Organometal halide perovskites as visible-light sensitizers for photovoltaic cells. *J. Am. Chem. Soc.* **2009**, *131*, 6050−6051.

(7) Park, N.-G.; Grätzel, M.; Miyasaka, T.; Zhu, K.; Emery, K. Towards stable and commercially available perovskite solar cells. *Nat. Energy* **2016**, *1*, 16152.

(8) Quan, L. N.; Rand, B. P.; Friend, R. H.; Mhaisalkar, S. G.; Lee, T.-W.; Sargent, E. H. Perovskites for next-generation optical sources. *Chem. Rev.* **2019**, *119*, 7444−7477.

(9) Yang, W. S.; Park, B.-W.; Jung, E. H.; Jeon, N. J.; Kim, Y. C.; Lee, D. U.; Shin, S. S.; Seo, J.; Kim, E. K.; Noh, J. H.; Seok, S. I. Iodide management in formamidinium-lead-halide-based perovskite layers for efficient solar cells. *Science* **2017**, *356*, 1376−1379.

(10) Chen, Q.; Wu, J.; Ou, X.; Huang, B.; Almutlaq, J.; Zhumekenov, A. A.; Guan, X.; Han, S.; Liang, L.; Yi, Z.; et al. All-inorganic perovskite nanocrystal scintillators. *Nature* **2018**, *561*, 88−93.

(11) Su, R.; Ghosh, S.; Liew, T. C. H.; Xiong, Q. Optical switching of topological phase in a perovskite polariton lattice. *Sci. Adv.* **2021**, *7*, No. eabf8049.

(12) Zhang, Q.; Diederichs, C.; Xiong, Q. Golden hour for perovskite photonics. *Photonics Res.* **2020**, *8*, PP1−PP4.

(13) Zhang, Q.; Shang, Q.; Su, R.; Do, T. T. H.; Xiong, Q. Halide Perovskite Semiconductor Lasers: Materials, Cavity Design, and Low Threshold. *Nano Lett.* **2021**, *21*, 1903−1914.

(14) Huang, C.; Zhang, C.; Xiao, S.; Wang, Y.; Fan, Y.; Liu, Y.; Zhang, N.; Qu, G.; Ji, H.; Han, J.; Ge, L.; Kivshar, Y.; Song, Q. Ultrafast control of vortex microlasers. *Science* **2020**, *367*, 1018−1021.

(15) Li, D.; Shi, J.; Xu, Y.; Luo, Y.; Wu, H.; Meng, Q. Inorganic-organic halide perovskites for new photovoltaic technology. *Natl. Sci. Rev.* **2018**, *5*, 559−576.

(16) Tang, B.; Hu, Y.; Dong, H.; Sun, L.; Zhao, B.; Jiang, X.; Zhang, L. An All-Inorganic Perovskite-Phase Rubidium Lead Bromide Nanolaser. *Angew. Chem., Int. Ed.* **2019**, *58*, 16134−16140.

(17) Zhang, H.; Wu, Y.; Liao, Q.; Zhang, Z.; Liu, Y.; Gao, Q.; Liu, P.; Li, M.; Yao, J.; Fu, H. A Two-Dimensional Ruddlesden-Popper

Perovskite Nanowire Laser Array based on Ultrafast Light-Harvesting Quantum Wells. *Angew. Chem., Int. Ed.* **2018**, *57*, 7748−7752.
(18) Han, P.; Luo, C.; Yang, S.; Yang, Y.; Deng, W.; Han, K. All-Inorganic Lead-Free 0D Perovskites by a Doping Strategy to Achieve a PLQY Boost from < 2% to 90%. *Angew. Chem., Int. Ed.* **2020**, *59*, 12709−12713.
(19) Yang, B.; Chen, J.; Hong, F.; Mao, X.; Zheng, K.; Yang, S.; Li, Y.; Pullerits, T.; Deng, W.; Han, K. Lead-Free, Air-Stable All-Inorganic Cesium Bismuth Halide Perovskite Nanocrystals. *Angew. Chem., Int. Ed.* **2017**, *56*, 12471−12475.
(20) Protesescu, L.; Yakunin, S.; Bodnarchuk, M. I.; Krieg, F.; Caputo, R.; Hendon, C. H.; Yang, R. X.; Walsh, A.; Kovalenko, M. V. Nanocrystals of cesium lead halide perovskites (CsPbX(3), X = Cl, Br, and I): novel optoelectronic materials showing bright emission with wide color gamut. *Nano Lett.* **2015**, *15*, 3692−3696.
(21) Kovalenko, M. V.; Protesescu, L.; Bodnarchuk, M. I. Properties and potential optoelectronic applications of lead halide perovskite nanocrystals. *Science* **2017**, *358*, 745−750.
(22) Akkerman, Q. A.; Rainò, G.; Kovalenko, M. V.; Manna, L. Genesis, challenges and opportunities for colloidal lead halide perovskite nanocrystals. *Nat. Mater.* **2018**, *17*, 394−405.
(23) Swarnkar, A.; Marshall, A. R.; Sanehira, E. M.; Chernomordik, B. D.; Moore, D. T.; Christians, J. A.; Chakrabarti, T.; Luther, J. M. Quantum dot-induced phase stabilization of alpha-$CsPbI_3$ perovskite for high-efficiency photovoltaics. *Science* **2016**, *354*, 92−95.
(24) Raino, G.; Becker, M. A.; Bodnarchuk, M. I.; Mahrt, R. F.; Kovalenko, M. V.; Stoferle, T. Superfluorescence from lead halide perovskite quantum dot superlattices. *Nature* **2018**, *563*, 671−675.
(25) Utzat, H.; Sun, W.; Kaplan, A. E. K.; Krieg, F.; Ginterseder, M.; Spokoyny, B.; Klein, N. D.; Shulenberger, K. E.; Perkinson, C. F.; Kovalenko, M. V.; Bawendi, M. G. Coherent single-photon emission from colloidal lead halide perovskite quantum dots. *Science* **2019**, *363*, 1068−1072.
(26) Ning, Z.; Gong, X.; Comin, R.; Walters, G.; Fan, F.; Voznyy, O.; Yassitepe, E.; Buin, A.; Hoogland, S.; Sargent, E. H. Quantum-dot-in-perovskite solids. *Nature* **2015**, *523*, 324−328.
(27) Chen, W.; Bhaumik, S.; Veldhuis, S. A.; Xing, G.; Xu, Q.; Gratzel, M.; Mhaisalkar, S.; Mathews, N.; Sum, T. C. Giant five-photon absorption from multidimensional core-shell halide perovskite colloidal nanocrystals. *Nat. Commun.* **2017**, *8*, 15198.
(28) Yan, F.; Xing, J.; Xing, G.; Quan, L.; Tan, S. T.; Zhao, J.; Su, R.; Zhang, L.; Chen, S.; Zhao, Y.; Huan, A.; Sargent, E. H.; Xiong, Q.; Demir, H. V. Highly Efficient Visible Colloidal Lead-Halide Perovskite Nanocrystal Light-Emitting Diodes. *Nano Lett.* **2018**, *18*, 3157−3164.
(29) Imran, M.; Caligiuri, V.; Wang, M.; Goldoni, L.; Prato, M.; Krahne, R.; De Trizio, L.; Manna, L. Benzoyl Halides as Alternative Precursors for the Colloidal Synthesis of Lead-Based Halide Perovskite Nanocrystals. *J. Am. Chem. Soc.* **2018**, *140*, 2656−2664.
(30) Gandini, M.; Villa, I.; Beretta, M.; Gotti, C.; Imran, M.; Carulli, F.; Fantuzzi, E.; Sassi, M.; Zaffalon, M.; Brofferio, C.; Manna, L.; Beverina, L.; Vedda, A.; Fasoli, M.; Gironi, L.; Brovelli, S. Efficient, fast and reabsorption-free perovskite nanocrystal-based sensitized plastic scintillators. *Nat. Nanotechnol.* **2020**, *15*, 462−468.
(31) Zhang, F.; Zhong, H.; Chen, C.; Wu, X.-g.; Hu, X.; Huang, H.; Han, J.; Zou, B.; Dong, Y. Brightly luminescent and color-tunable colloidal $CH_3NH_3PbX_3$ (X= Br, I, Cl) quantum dots: potential alternatives for display technology. *ACS Nano* **2015**, *9*, 4533−4542.
(32) Yakunin, S.; Protesescu, L.; Krieg, F.; Bodnarchuk, M. I.; Nedelcu, G.; Humer, M.; De Luca, G.; Fiebig, M.; Heiss, W.; Kovalenko, M. V. Low-threshold amplified spontaneous emission and lasing from colloidal nanocrystals of caesium lead halide perovskites. *Nat. Commun.* **2015**, *6*, 8056.
(33) Xu, Y.; Chen, Q.; Zhang, C.; Wang, R.; Wu, H.; Zhang, X.; Xing, G.; Yu, W. W.; Wang, X.; Zhang, Y.; Xiao, M. Two-photon-pumped perovskite semiconductor nanocrystal lasers. *J. Am. Chem. Soc.* **2016**, *138*, 3761−3768.
(34) Tong, Y.; Bladt, E.; Ayguler, M. F.; Manzi, A.; Milowska, K. Z.; Hintermayr, V. A.; Docampo, P.; Bals, S.; Urban, A. S.; Polavarapu, L.; Feldmann, J. Highly luminescent cesium lead halide perovskite nanocrystals with tunable composition and thickness by ultrasonication. *Angew. Chem., Int. Ed.* **2016**, *55*, 13887−13892.
(35) Wang, Y.; Li, X.; Zhao, X.; Xiao, L.; Zeng, H.; Sun, H. Nonlinear Absorption and Low-Threshold Multiphoton Pumped Stimulated Emission from All-Inorganic Perovskite Nanocrystals. *Nano Lett.* **2016**, *16*, 448−453.
(36) Wang, Y.; Li, X.; Song, J.; Xiao, L.; Zeng, H.; Sun, H. All-Inorganic Colloidal Perovskite Quantum Dots: A New Class of Lasing Materials with Favorable Characteristics. *Adv. Mater.* **2015**, *27*, 7101−7108.
(37) Wang, L.; Meng, L.; Chen, L.; Huang, S.; Wu, X.; Dai, G.; Deng, L.; Han, J.; Zou, B.; Zhang, C.; Zhong, H. Ultralow-Threshold and Color-Tunable Continuous-Wave Lasing at Room-Temperature from In Situ Fabricated Perovskite Quantum Dots. *J. Phys. Chem. Lett.* **2019**, *10*, 3248−3253.
(38) Wu, K.; Park, Y. S.; Lim, J.; Klimov, V. I. Towards zero-threshold optical gain using charged semiconductor quantum dots. *Nat. Nanotechnol.* **2017**, *12*, 1140−1147.
(39) Nagamine, G.; Rocha, J. O.; Bonato, L. G.; Nogueira, A. F.; Zaharieva, Z.; Watt, A. A.; de Brito Cruz, C. H.; Padilha, L. A. Two-photon absorption and two-photon-induced gain in perovskite quantum dots. *J. Phys. Chem. Lett.* **2018**, *9*, 3478−3484.
(40) Zhao, W.; Qin, Z.; Zhang, C.; Wang, G.; Huang, X.; Li, B.; Dai, X.; Xiao, M. Optical gain from biexcitons in $CsPbBr_3$ nanocrystals revealed by two-dimensional electronic spectroscopy. *J. Phys. Chem. Lett.* **2019**, *10*, 1251−1258.
(41) Wang, Y.; Zhi, M.; Chang, Y.-Q.; Zhang, J.-P.; Chan, Y. Stable, Ultralow Threshold Amplified Spontaneous Emission from CsPbBr3 Nanoparticles Exhibiting Trion Gain. *Nano Lett.* **2018**, *18*, 4976−4984.
(42) Sugawara, M.; Hatori, N.; Ishida, M.; Ebe, H.; Arakawa, Y.; Akiyama, T.; Otsubo, K.; Yamamoto, T.; Nakata, Y. Recent progress in self-assembled quantum-dot optical devices for optical telecommunication: temperature-insensitive 10 Gb s^{-1} directly modulated lasers and 40 Gb s^{-1} signal-regenerative amplifiers. *J. Phys. D: Appl. Phys.* **2005**, *38*, 2126−2134.
(43) Kim, S.; Wang, Y.; Keever, M.; Harris, J. High-frequency modulation characteristics of 1.3-μm InGaAs quantum dot lasers. *IEEE Photonics Technol. Lett.* **2004**, *16*, 377−379.
(44) Rinehart, J. D.; Schimpf, A. M.; Weaver, A. L.; Cohn, A. W.; Gamelin, D. R. Photochemical Electronic Doping of Colloidal CdSe Nanocrystals. *J. Am. Chem. Soc.* **2013**, *135*, 18782−18785.
(45) Wang, C.; Wehrenberg, B. L.; Woo, C. Y.; Guyot-Sionnest, P. Light emission and amplification in charged CdSe quantum dots. *J. Phys. Chem. B* **2004**, *108*, 9027−9031.
(46) Kozlov, O. V.; Park, Y.-S.; Roh, J.; Fedin, I.; Nakotte, T.; Klimov, V. I. Sub−single-exciton lasing using charged quantum dots coupled to a distributed feedback cavity. *Science* **2019**, *365*, 672−675.
(47) Kobiyama, E.; Tahara, H.; Sato, R.; Saruyama, M.; Teranishi, T.; Kanemitsu, Y. Reduction of Optical Gain Threshold in CsPbI3 Nanocrystals Achieved by Generation of Asymmetric Hot-Biexcitons. *Nano Lett.* **2020**, *20*, 3905−3910.
(48) Yu, J.; Shendre, S.; Koh, W.-k.; Liu, B.; Li, M.; Hou, S.; Hettiarachchi, C.; Delikanli, S.; Hernández-Martínez, P.; Birowosuto, M. D.; et al. Electrically control amplified spontaneous emission in colloidal quantum dots. *Sci. Adv.* **2019**, *5*, No. eaav3140.
(49) Wang, H.; Guerrero, A.; Bou, A.; Al-Mayouf, A. M.; Bisquert, J. Kinetic and material properties of interfaces governing slow response and long timescale phenomena in perovskite solar cells. *Energy Environ. Sci.* **2019**, *12*, 2054−2079.
(50) Deng, X.; Wen, X.; Lau, C. F. J.; Young, T.; Yun, J.; Green, M. A.; Huang, S.; Ho-Baillie, A. W. Y. Electric field induced reversible and irreversible photoluminescence responses in methylammonium lead iodide perovskite. *J. Mater. Chem. C* **2016**, *4*, 9060−9068.
(51) Yuan, Y.; Huang, J. Ion migration in organometal trihalide perovskite and its impact on photovoltaic efficiency and stability. *Acc. Chem. Res.* **2016**, *49*, 286−293.
(52) Zhang, H.; Fu, X.; Tang, Y.; Wang, H.; Zhang, C.; Yu, W. W.; Wang, X.; Zhang, Y.; Xiao, M. Phase segregation due to ion migration in

https://doi.org/10.1021/acs.nanolett.1c02880
Nano Lett. 2021, 21, 7831−7838

all-inorganic mixed-halide perovskite nanocrystals. *Nat. Commun.* **2019**, *10*, 10881088.
(53) Yi, H. T.; Rangan, S.; Tang, B.; Frisbie, C. D.; Bartynski, R. A.; Gartstein, Y. N.; Podzorov, V. Electric-field effect on photoluminescence of lead-halide perovskites. *Mater. Today* **2019**, *28*, 31−39.
(54) Sharma, D. K.; Hirata, S.; Biju, V.; Vacha, M. Stark effect and environment-induced modulation of emission in single halide perovskite nanocrystals. *ACS Nano* **2019**, *13*, 624−632.
(55) Makarov, N. S.; Guo, S.; Isaienko, O.; Liu, W.; Robel, I.; Klimov, V. I. Spectral and dynamical properties of single excitons, biexcitons, and trions in cesium-lead-halide perovskite quantum dots. *Nano Lett.* **2016**, *16*, 2349−2362.
(56) Yin, C.; Chen, L.; Song, N.; Lv, Y.; Hu, F.; Sun, C.; Yu, W. W.; Zhang, C.; Wang, X.; Zhang, Y.; Xiao, M. Bright-Exciton Fine-Structure Splittings in Single Perovskite Nanocrystals. *Phys. Rev. Lett.* **2017**, *119*, 026401.
(57) Liu, Y.; Wang, J.; Zhang, L.; Liu, W.; Wu, C.; Liu, C.; Wu, Z.; Xiao, L.; Chen, Z.; Wang, S. Exciton and bi-exciton mechanisms in amplified spontaneous emission from CsPbBr3 perovskite thin films. *Opt. Express* **2019**, *27*, 29124−29132.
(58) Huang, X.; Chen, L.; Zhang, C.; Qin, Z.; Yu, B.; Wang, X.; Xiao, M. Inhomogeneous Biexciton Binding in Perovskite Semiconductor Nanocrystals Measured with Two-Dimensional Spectroscopy. *J. Phys. Chem. Lett.* **2020**, *11*, 10173−10181.
(59) Nakahara, S.; Tahara, H.; Yumoto, G.; Kawawaki, T.; Saruyama, M.; Sato, R.; Teranishi, T.; Kanemitsu, Y. Suppression of trion formation in $CsPbBr_3$ perovskite nanocrystals by postsynthetic surface modification. *J. Phys. Chem. C* **2018**, *122*, 22188−22193.
(60) Empedocles, S. A.; Bawendi, M. G. Quantum-confined stark effect in single CdSe nanocrystallite quantum dots. *Science* **1997**, *278*, 2114−2117.
(61) Seufert, J.; Obert, M.; Scheibner, M.; Gippius, N. A.; Bacher, G.; Forchel, A.; Passow, T.; Leonardi, K.; Hommel, D. Stark effect and polarizability in a single CdSe/ZnSe quantum dot. *Appl. Phys. Lett.* **2001**, *79*, 1033−1035.

https://doi.org/10.1021/acs.nanolett.1c02880
Nano Lett. 2021, 21, 7831−7838